

Supporting Information

Preparation and corrosion inhibition mechanism of a Chitosan
ion liquid Schiff base for protection of N80 in HCl solution

Miantuo Li^{1,2}, Fengting Li^{1,2}, Jianwen Hu^{1,2}, Nannan Cui^{1,2}, Huiling Su^{1,2}, Lizhi Li^{1,2},
Zhikun Wang^{1,2,*}, Shuangqing Sun^{1,2}, Songqing Hu^{1,2,*}

¹ *School of Materials Science and Engineering, China University of Petroleum (East China), Qingdao 266580, PR China*

² *Institute of Advanced Materials, China University of Petroleum (East China), Qingdao 266580, PR China*

As shown in Fig. S1 and Table S1, the molecular weight of CS ($M_n=3000$) is increased after the ionic liquidization and the Schiff alkalization, which is mainly due to the introduction of PTSA and Schiff base groups on the molecular chain of CS. Among three CS-IL-SBs inhibitors, the molecular weight of CS-IL-Vin is the largest, possibly because more vanilla groups are grafted to CS-IL.

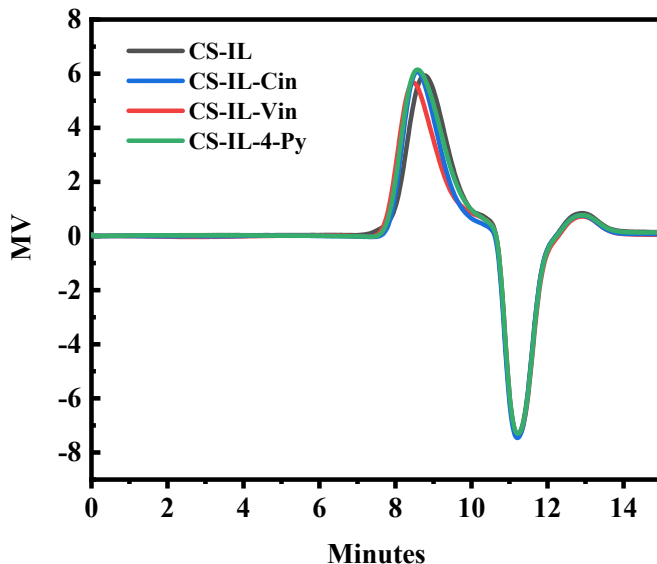


Fig S1. Outflow curves of the obtained CS-IL and CS-IL-SBs

Table S1. Molecular weight tests of the obtained CS-IL and CS-IL-SBs

Distribution Name	Mn (Daltons)	MP (Daltons)
CS-IL	3329	7358
CS-IL-Cin	5280	10429
CS-IL-Vin	6177	12860
CS-IL-4-Py	4646	10293

Table S2. Comparative table of Chitosan Schiff base corrosion inhibitors

Chitosan Schiff base corrosion inhibitors	Corrosive environment	Concentration	Corrosion inhibition efficiency	reference
Our products	15% HCl solution	400mg/L	93.45%	
Chitosan cinnamaldehyde	15% HCl solution	400mg/L	85.16%	[1]
Chitosan thiophene carboxaldehyde	1 M HCl solution	1500ppm	92%	[2]
Chitosan salicylaldehyde	1 M HCl solution	1500ppm	91%	[3]
Chitosan vanillin	1 M HCl solution	1500ppm	91.1%	[4]
Chitosan benzaldehyde	1 M HCl solution	800mg/L	87.11%	[5]
Salicylaldehyde-Chitosan	3.5% NaCl solution	150mg/L	95.2%	[6]
Chitosan 4-pyridinecarboxaldehyde-CuO	3.5% NaCl solution	200ppm	94.5%	[7]
Chitosan vanillin-ZnO	3.5% NaCl solution	200ppm	95.96%	[8]

Fig. S2 indicates the thermogravimetric analysis (TGA) of pristine CS and its corresponding CS-IL and CS-IL-SBs. For CS, the first thermal degradation occurs at 110 °C, with a weight loss of 9 % attributed to the loss of water molecules. While the second thermal loss starts around 250 °C and exhibits a mass loss of 33 % at 310 °C. This is caused by the thermal degradation of the pyranose ring on CS, which resulted in the broken of the glycosidic linkages between *N*-acetylglucosamine rings and glucosamine, and the release of volatile compounds. CS-IL undergoes three thermal degradations, the first and second thermal degradations are consistent with that of CS. While the third thermal loss starts around 312 °C and exhibits a mass loss of 28 % at 406 °C. This is caused by the thermal degradation of the PTSA. For CS-IL-SBs, all polymers undergo three major thermal degradation steps. The first decomposition step is due to loss of water molecule. The second degradation step occurring in the range of 220 °C–310 °C is due to depolymerization of Schiff bases. While the third thermal loss occurs in the range of 340 °C–430 °C. This is caused by the thermal degradation of PTSA. Because of the Schiff base group grafted on CS-IL, the pyrolysis temperature of PTSA group may increase, and the pyrolysis curve of CS-IL-SBs may shift to the right. The main thermal degradation step of CS-IL-SBs indicates that ionic liquid Schiff base polymer is more stable than CS. The stability of the ionic liquid Schiff base polymer compared to CS may be due to the grafting of PTSA and aldehyde groups on the CS matrix.

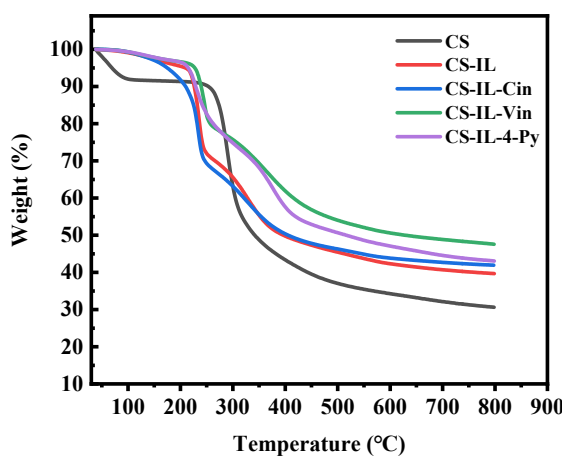


Fig. S2 Thermogravimetric analysis (TGA) of pristine CS and its corresponding CS-IL and CS-IL-SBs

Fig. S3 provides the X-ray diffraction (XRD) examination of pristine CS and its corresponding CS-IL and CS-IL-SBs. As shown in Fig S3, the XRD of pure CS and CS derivatives are similar and exhibit peak at the 2θ diffraction angle of 20° . The reason for this is that CS has a significant number of OH groups in its repeating units, which are highly polar and enable the formation of a large number of inter- and intra-molecular hydrogen bonds. In comparison to pure CS, CS-IL and CS-IL-SBs have less intense and much broader peaks, indicating that grafting CS with PTSA and Schiff base groups deform the crystal zone in the CS system, making it less crystalline.⁹

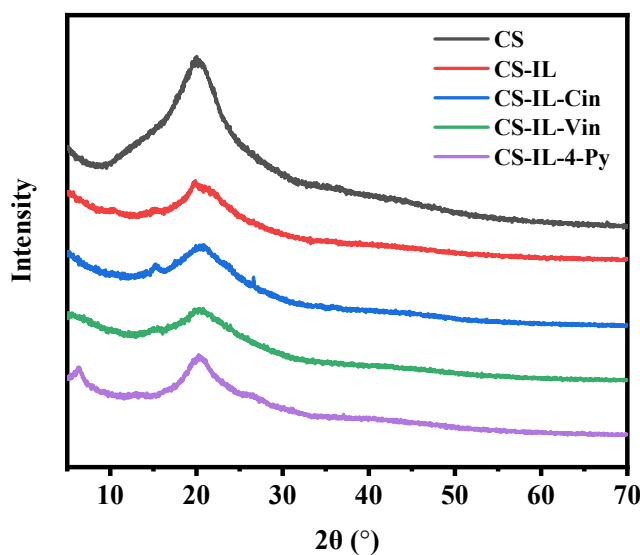


Fig. S3 X-ray diffraction (XRD) tests of pristine CS and its corresponding CS-IL and CS-IL-SBs

Zeta potential is an important indicator to characterize the stability of as-prepared CS-IL-SBs solution (Fig. S4). In general, the smaller the absolute value of zeta potential is, the worse the stability of dispersion system is. It could be seen that the zeta potentials of as-prepared CS-IL-SBs in 15% HCl solution are positive, indicating that the surfaces of CS-IL-SBs are positively charged. With the introduction of Schiff base groups into CS-IL, the value of zeta potential has been increased, indicating that the dispersion of CS-IL is improved in 15% HCl solution. Among three CS-IL-SBs inhibitors, the CS-IL-Vin inhibitor presents the highest value of zeta potential, suggesting the best stability in 15% HCl solution. CS-IL-SBs show high value of zeta potential in 15% HCl solution because the introduction of PTSA and Schiff base groups can improve the stability of corrosion inhibitor molecules.

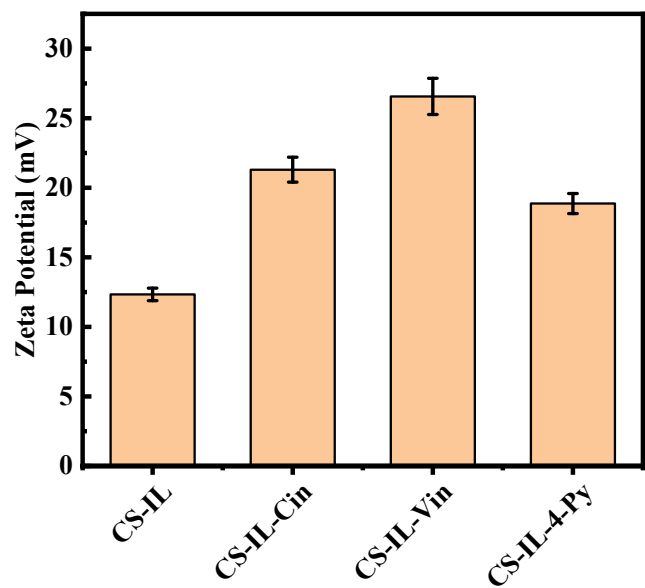


Fig. S4 Zeta potential tests of synthesized CS-IL and CS-IL-SBs

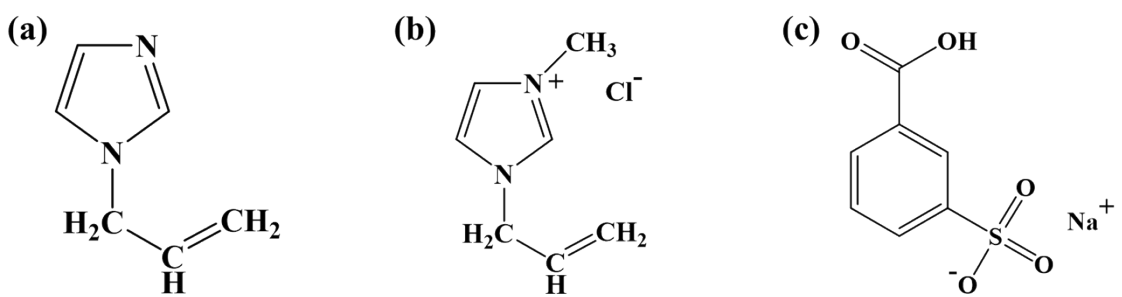


Fig. S5 Molecular structure formula of three compound auxiliaries, (a) 1-allylimidazole, (b) 1-allyl-3-methylimidazole chloride, and (c) sodium 3-carboxybenzene sulfonate.

Fig. S6 displays the corresponding contact angle (CA) of the investigated N80 steel surfaces with and without the addition of corrosion inhibitors. It's clear that the value of CA can be increased after introducing CS-IL-SBs into 15% HCl solution, which further indicate that the adsorbed CS-IL-SBs film could impede the contact of water to N80 steel surface. Thus, the corrosion of metal will be inhibited.

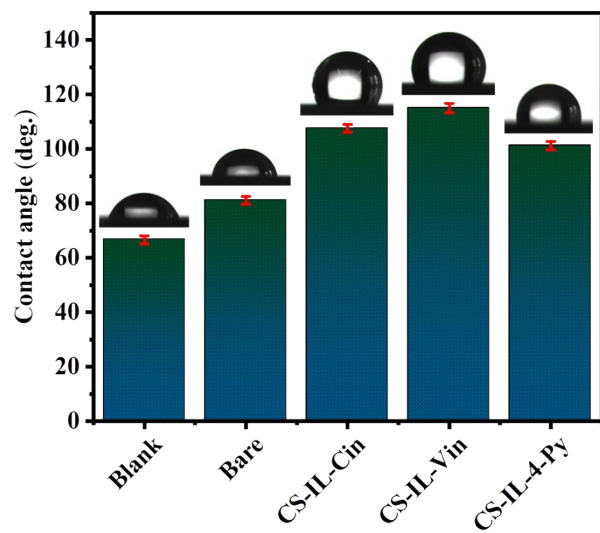


Fig. S6 Contact angle tests of the steel before and after treatment of CS-IL-SBs

Table S3. Thermodynamic parameters of adsorption isotherm.

Inhibitor	R ²	Slope	K _{ads}	ΔG _{ads} ⁰ (kJ/mol)
CS	0.99927	0.01676	59.67	-20.081
CS-IL	0.99989	0.01579	63.33	-20.228
CS-IL-Cin	0.99341	0.01118	89.44	-21.084
CS-IL-Vin	0.98421	0.01119	89.37	-21.082
CS-IL-4-Py	0.99934	0.01328	75.30	-20.658

Table S4. EIS fitted electrochemical parameters for the N80 steel in 15% HCl solution containing different concentrations of CS-IL-SBs at 298 K.

Inhibitors	Concentration (mg/L)	R_s (Ω/cm^2)	f	Y_0 (10^{-6} S.Seen/ cm^2)	n	CPE_{dl}	R_{ct} (Ω/cm^2)	η (%)
blank	0	0.7089	21.65	280.5	0.8166	113.93	45.21	-
CS-IL-Cin	50	0.3035	24.93	242.4	0.7619	72.77	115.6	60.9
	100	0.5780	12.40	168.6	0.7827	65.43	173.7	74.0
	200	0.9118	7.94	129.9	0.7945	58.17	273.8	83.5
	300	0.8241	7.94	137.8	0.7765	57.51	342.3	86.8
	400	0.9567	5.00	142.9	0.7845	67.98	422.0	89.3
CS-IL-Vin	50	1.064	106.8	183.1	0.8448	66.68	245.8	81.6
	100	1.161	235.5	150.9	0.8195	40.41	458.7	90.1
	200	1.334	218.3	138.7	0.8814	58.88	461.1	90.2
	300	1.229	263.1	141.6	0.8232	38.20	578.7	92.2
	400	1.212	450.1	102.7	0.8727	37.34	916.1	95.1
CS-IL-4-Py	50	0.7146	31.25	184.9	0.8819	99.11	55.94	19.2
	100	0.7466	12.40	173.7	0.8438	87.97	126.7	64.3
	200	0.6385	9.93	142.3	0.8383	72.93	188.7	76.0
	300	0.6518	15.63	170.7	0.8430	83.07	125.4	63.9
	400	0.6007	15.62	140.1	0.8415	67.72	137.6	67.1

Table S5. Fitted electrochemical parameters from polarization curves tests for the N80 steel in 15% HCl solution containing different concentrations of CS-IL-SBs.

Inhibitor	Conc. (mg/L)	β_a (mV/dec)	$-\beta_c$ (mV/dec)	E_{corr} (mV/SCE)	I_{corr} ($\mu\text{A}/\text{cm}^2$)	η (%)
blank	—	80.3	76.8	-426	380.0	—
	50	128.6	115	-452	151.5	60.14
	100	112.4	113	-452	125.5	66.97
CS-IL-Cin	200	120.0	124.3	-450	105.2	72.31
	300	124.9	115	-451	89.3	76.51
	400	122.9	102.1	-446	66.8	82.43
	50	106.1	105.6	-438	150.2	60.48
	100	126.1	107.3	-453	125.4	66.99
CS-IL-Vin	200	159.2	106.2	-456	100.4	73.58
	300	138.6	129.9	-458	76.7	79.82
	400	121.7	119.4	-457	54.1	85.76
	50	70.8	81.1	-425	148.7	60.87
	100	98.4	79.2	-431	121.1	68.14
CS-IL-4-Py	200	78.6	77.2	-428	100.5	73.54
	300	133.7	87.3	-432	83.9	77.93
	400	91.8	42.4	-437	78.4	79.38

Table S6. Laser confocal micro-morphology roughness parameters of the N80 steel after corrosion in 15% HCl solution without or with 400 mg/L CS-IL- SBs at 298

K for 24 h.

	S _z (μm)	S _a (μm)	S _{tr}	S _{pc} (1/mm)
Blank	0.447	5.645	0.765	649.968
CS-IL-Cin	0.395	4.550	0.534	595.829
CS-IL-Vin	0.311	3.829	0.076	499.279
CS-IL-4-Py	0.407	4.764	0.110	624.087

Table S7. Global activity parameters of CS-IL and CS-IL-SBs corrosion inhibitors.

Inhibitor	μ/eV	η/eV	$S/(1/\text{eV})$	ω/eV	ΔN
CS-IL	-2.946	2.181	0.458	1.990	0.929
CS-IL-Cin	-3.931	1.459	0.685	5.296	1.052
CS-IL-Vin	-3.978	1.192	0.839	6.638	1.268
CS-IL-4-Py	-3.075	1.597	0.626	2.960	1.229

Table S8. Fukui indices of CS-IL and CS-IL-SBs corrosion inhibitors.

CS-IL			CS-IL-Cin			CS-IL-Vin			CS-IL-4-Py		
Atom	$f(\vec{r})^+$	$f(\vec{r})^-$	Atom	$f(\vec{r})^+$	$f(\vec{r})^-$	Atom	$f(\vec{r})^+$	$f(\vec{r})^-$	Atom	$f(\vec{r})^+$	$f(\vec{r})^-$
O1	0.004	0.012	O3	0.018	0.046	N8	0.100	0.051	N8	0.110	0.005
N9	0.000	0.084	N8	0.080	0.002	C22	0.102	0.020	S28	0.001	0.046
N31	0.003	0.001	O13	0.017	0.009	C23	0.038	0.051	O29	0.006	0.128
N54	0.005	0.065	C22	0.075	0.009	C24	0.053	0.046	O30	0.005	0.113
S77	0.020	0.029	C23	0.069	0.007	C25	0.040	0.035	O31	0.002	0.099
O78	0.027	0.071	C24	0.090	0.012	C26	0.066	0.050	C40	0.095	0.004
O79	0.027	0.063	C25	0.020	0.002	C27	0.032	0.044	C41	0.057	0.002
O80	0.037	0.077	C26	0.041	0.007	C28	0.045	0.024	C42	0.056	0.004
			C27	0.036	0.008	O29	0.058	0.072	C43	0.065	0.008
			C28	0.068	0.014	O30	0.021	0.042	N44	0.102	0.025
			C29	0.038	0.007	N68	0.001	0.000	C45	0.056	0.008
			C30	0.040	0.006	S92	0.002	0.014	C46	0.065	0.005
			S45	0.001	0.043	O93	0.003	0.034	N80	0.001	0.007
			O46	0.005	0.101	O94	0.001	0.031			
			O47	0.002	0.107	O95	0.001	0.039			
			O48	0.000	0.115						
			N85	0.001	0.002						

References

- 1 D. S. Chauhan, M. A. J. Mazumder, M. A. Quraishi and K. R. Ansari, Chitosan-cinnamaldehyde Schiff base: A bioinspired macromolecule as corrosion inhibitor for oil and gas industry, *Int. J. Biol. Macromol.*, 2020, **158**, 127–138.
- 2 R. Menaka and S. Subhashini, Chitosan Schiff base as effective corrosion inhibitor for mild steel in acid medium, *Polym. Int*, 2016, **66**, 349–358.
- 3 R. Menaka and S. Subhashini, Chitosan Schiff base as eco-friendly inhibitor for mild steel corrosion in 1 M HCl, *J Adhes Sci Technol*, 2016, **66**, 349–358.
- 4 M. Ramanathan, G. Rajendran and S. Sethumanickam, Eco-friendly chitosan vanillin Schiff base as anti-corrosive agent for mild steel in 1 M HCl and as scale inhibitor for CaCO₃, *J. Adhes. Sci Technol*, 2022, **36**, 2588–2611.
- 5 J. Wu, J. Wu, L. L. Lu and P. Mei, 8-Hydroxyquinoline-functionalized chitosan Schiff base as an efficient and environmentally friendly corrosion inhibitor for N80 steel in acidic environments, *J. Appl. Polym. Sci.*, 2023, **140**, e54073.
- 6 K. P. Ansari, D. D. Chauhan, M. A. Quraishi and A. J. Mohammad, Chitosan Schiff base: an environmentally benign biological macromolecule as a new corrosion inhibitor for oil & gas industries, *Int. J. Biol. Macromol.*, 2020, **144**, 305–315.
- 7 C. Verma, M. A. Quraishi, A. Alfantazi and K. Y. Rhee, Corrosion inhibition potential of chitosan based Schiff bases: Design, performance and applications, *Inte. J. Biol. Macromol.*, 2021, **184**, 135–143.
- 8 H. L. Liu, Z. M. Zhu, J. F. Hu, X. Lai, J. Q. Qu, Inhibition of Q235 corrosion in sodium chloride solution by chitosan derivative and its synergistic effect with ZnO, *Carbohydr. Polym.*, 2022, **296**, 119936.
- 9 S. N. Dalhatu, K. N. Modu, A. A. Mahmoud, Z. U. Zango, A. B. Umar, F. Usman, J. O. Dennis, A. Alsadig, K. H. Ibnaouf and O. A. Aldaghri, L-arginine grafted chitosan as corrosion inhibitor for mild steel protection, *Polymers*, 2023, **15**, 398.